Check for updates

# A novel photothermo-responsive nanocarrier for the controlled release of low-volatile fragrances†

Sihang Wang,[a] Dong Jiang,[a] Zhuxian Zhou, [iD][b] Youqing Shen [iD][b] and Liming Jiang [iD] *[a]

We herein present a facile approach to create polydopamine (PDA) modified silica-based nanocarriers for use in the encapsulation and photothermally responsive release of the synthetic sandalwood odorant Sandalore (SA) as a low-volatile model fragrance. The method involves impregnating mesoporous silica nanoparticles with an ethanol solution of SA followed by surface functionalization *via* the *in situ* self-polymerization of dopamine under alkaline conditions. The resulted nanocomposites have high fragrance loading capacity with up to ~85% by weight of SA relative to the silica matrix and are capable of effectively preserving the cargo in the dark or indoors. The aroma release was significantly accelerated upon illumination due to the photothermal heating effect of the PDA shell, which is proportional to the coating content and the irradiation intensity. Additionally, the emulated laundry tests showed that the composites exhibited a higher deposition efficiency on the fabric surface and better washing-resistance as compared to the control particles without PDA coating.

## 1. Introduction

Sandalore®, a synthetic odorant, is widely used in the perfumery industries due to its sweet and warm smell similar to natural sandalwood oil.[1–3] Recent studies have also shown that this terpenoid compound may have potential therapeutic effects in the promotion of wound healing and the stimulation of hair growth.[4–6] However, unlike most flavors and fragrances, Sandalore is low-volatile with a saturated vapor pressure as low as of $8.3 \times 10^{-4}$ Pa at 25 °C.[7] The poor volatilization may adversely affect its usefulness, such as being unable to reach the desired olfactory threshold in certain cases. Besides, this viscous oily liquid is usually not conducive to aromatic finishing in aqueous media without additional surfactants.[8] One promising solution to these problems is to fabricate a suitable delivery system for the controlled release of Sandalore, which will contribute to broadening its practical applications.

Over the last decade, the development of flavor and fragrance nanocapsules has drawn extensive attention in academia and industry.[9–13] In this regard, porous silica-based materials are particularly attractive as a matrix for encapsulation of fragrant molecules,[14–19] because they offer inherent advantages over the commonly used polymers, such as high mechanical resistance, excellent biocompatibility, and great loading capacity.[14] For example, Zhu *et al.* employed mesoporous silica nanoparticles (MSNs) modified with polyelectrolytes to enclose hydrophilic perfume, which improved the loading content of fragrance and long-lasting effects.[17] Cao and coworkers prepared silica nano-capsules containing spices through an interfacial sol–gel process of tetraethylorthosilicate in oil/water miniemulsions.[18] Incorporation of the nanocapsules into polyacrylate latexes produced a composite film that could release fragrances sustainably. Recently, Zhang's group developed azobenzene-modified silica nanorods as a photoresponsive carrier for fragrance delivery, where the aroma release was tuned by the *cis–trans* isomerization of the azo linkage induced by UV irradiation.[19]

Polydopamine (PDA) is a mimic of the specialized adhesive foot protein Mefp-5 secreted from mussels, which has been proven to be capable of firmly attaching to most organic and inorganic variant substances, including polymers, metals, oxides, and ceramics.[20,21] The melanin-like polymer is also a novel photothermal agent in clinical therapy that can efficiently absorb and transfer optical energy into heat.[22–24] With these attractive properties, PDA and its derivatives have shown great potential in a wide range of applications across the biomedical, and materials sciences, as well as in the applied engineering and technology fields.[25–31] For example, Cai *et al.* recently reported a new kind of PDA-based porous nanoparticles as a drug carrier for synergistic thermo-chemotherapy, therein a significant promotion effect of near-infrared irradiation on the drug release was observed.[29]

[a]Key Laboratory of Macromolecular Synthesis and Functionalization of Ministry of Education, Department of Polymer Science and Engineering, Zhejiang University, Hangzhou 310027, China. E-mail: cejlm@zju.edu.cn

[b]Key Laboratory of Biomass Chemical Engineering of Ministry of Education, Center for Bionanoengineering, College of Chemical and Biological Engineering, Zhejiang University, Hangzhou 310027, China

† Electronic supplementary information (ESI) available. See DOI: 10.1039/c9ra10662f

In the present work, we chose Sandalore as the model compound and designed a photothermo-responsive nano-carrier for the encapsulation and controlled release of low volatile fragrances. Herein, the fragrance oil was first loaded into the silica cage and further blocked by the PDA film *in situ* formed on the particle surface. The PDA possesses plentiful polar groups such as catechol, amine, and imine moieties, available for hydrogen bonding interactions with entrapped molecules,[32,33] which would lead to increased diffusion barrier of the payload. More importantly, the surface coating will act as a switch to modulate the aroma volatilization *via* responding to light stimulus. In other words, the nanocomposites would be triggered by light where the PDA absorbs the light and converts it into heat thereby liberating loaded fragrances. Moreover, the PDA coating may afford the nanoparticles favorable affinity responsible for compatibility with the other ingredients of household/personal care products. Despite significant interest in the stimuli-responsive fragrance release systems,[11–13] photo-thermally sensitive materials as delivery vehicles for fragrances have not previously been explored to the best of our knowledge.

## 2. Experimental

### 2.1. Materials

Sandalore® (SA, 5-(2,2,3-trimethyl-3-cyclopentenyl)-3-methyl-pentan-2-ol) with 92.0% purity was provided by Dayangchem Co., Ltd. (Hangzhou, China) and used after distillation. Tetraethyl orthosilicate (TEOS, 99.9%), cetyltrimethylammonium bromide (CTAB, 99.0%), dopamine hydrochloride (99.0%), tris(hydroxymethyl)aminomethane (Tris, 99.5%), and other chemicals of analytical grade were purchased from Sinopharm Chemical Reagent Co. (Shanghai, China). Deionized water was used throughout this work.

### 2.2. Preparation of Sandalore-loaded mesoporous silica nanoparticles covered with polydopamine (SA/MSN@PDA)

**2.2.1. Synthesis of mesoporous silica nanoparticles (MSNs).** MSNs were synthesized according to the reported method with a slight modification.[34] CTAB 1.0 g was dissolved in 480 mL of deionized water and then mixed with 3.0 mL of aqueous NaOH (2.0 mol $L^{-1}$). The mixture was vigorously stirred at 80 °C for 2 h. Then, 5.0 mL of TEOS was added to the resulting solution dropwise and refluxed for 2 h. After cooled to room temperature, the dispersion was centrifuged at 8000 rpm for 5 min (the diameter of the centrifuge rotor = 18.4 cm), the supernatant was discarded and the precipitate was collected. The product was washed thoroughly with water and ethanol and dried under vacuum overnight. Finally, the powder sample was calcined at 550 °C in air for 5 h to remove the surfactant template (CTAB).

**2.2.2. Loading of Sandalore in MSNs and post-modification with PDA.** Sandalore (SA) was prepared into an ethanol solution (50 mg $mL^{-1}$) in advance, and then 400 mg MSNs were added to 8 mL of the solution. The mixture was stirred for 3 h at room temperature, and subjected to vacuum for removal of solvent to give the desired composite. The sample

contained SA that accounted for 46% of the total mass, which will hereafter be referred to as denoted as $SA_{46}$/MSN.

To a 20 mL solution of dopamine hydrochloride (0.125, 0.25, or 0.5 mg $mL^{-1}$) in Tris buffer (10 mM, pH 8.5), $SA_{46}$/MSN (374 mg) was added and the suspension was stirred for 6 h at room temperature. Once the polymerization was finished, the PDA-covered particles were collected by centrifugation (8000 rpm, 10 min; the diameter of the centrifuge rotor = 18.4 cm) and then washed twice alternately with water and ethanol to remove loose deposits.

The loading content (LC) and encapsulation efficiency (EE) of Sandalore in the nanoparticles (NPs) were calculated by the following equations based on thermogravimetric and elemental analyses (see the ESI† for details).

$$\text{LC (\%)} = W_{\text{SA in NP}}/W_{\text{NP}} \times 100\%$$

$$\text{EE (\%)} = W_{\text{SA in NP}}/W_{\text{total SA}} \times 100\%$$

where $W_{\text{NP}}$, $W_{\text{SA in NP}}$, and $W_{\text{total SA}}$ were the weights of the NP SA/MSN@PDA, SA in NP, and total SA, respectively.

### 2.3. Preparation of the control samples

For comparison, PDA-coated MSNs that do not contain Sandalore (labeled as MSN@PDA) were prepared with the same procedure for SA/MSN@PDA except the pure MSN instead of $SA_{46}$/MSN.

Polydopamine was synthesized following a previously reported method.[32] To a Tris buffer solution (pH = 8.5, 100 mL) was added 0.5 g dopamine hydrochloride, and the resulting mixture was stirred for 12 h in an atmosphere of air at room temperature. After the reaction completion, PDA suspensions were collected by centrifugation (8000 rpm), washed three times with water and dried in a vacuum for 24 h.

### 2.4. Characterization of the nanoparticles

Thermogravimetric analysis (TGA) was conducted on a Q50 thermogravimetric analyzer (TA Instruments, New Castle, USA) with a heating rate of 15°C $min^{-1}$ in airflow. Elemental analysis (EA) was performed on a Vario EL (Elementaranalysen GmbH, Germany) using standard conditions. Particle size and zeta potential were measured using a Malvern Mastersizer 2000 (Malvern Instruments Ltd., UK) at room temperature under the scattering angle of 90° at a wavelength of 633 nm. Before the measurement, the samples were suspended in deionized 100 mL of water (1.0 mg $mL^{-1}$), and then sonicated in 40 Hz for 10 min and then placed into a polystyrene cuvette. The data were given as the average of three measurements. The surface morphology of nanoparticles was observed by an S4800 field-emission scanning electron microscopy (Hitachi, Japan) after sputtering with platinum at an accelerating voltage of 3 kV. The particle size was analyzed using the scanning electron microscope (SEM) images by the Nano Measure software (Version 1.2.5) and expressed as a mean ± standard deviation based on 200 random measurements. Transmission electron microscopy (TEM) images were taken using an HT7700 transmission

electron microscope (Hitachi, Japan) operated at an acceleration voltage of 120 kV. The samples for TEM were suspended in deionized water and drop-casted on a copper grid coated with carbon membrane. The grid was allowed to dry at ambient before characterization. Nitrogen physisorption measurements were carried out at 77 K on a BELSORP-max automated gas sorption apparatus (MicrotracBEL Corp., Japan). Before the measurement, samples (20–30 mg) were degassed under vacuum ($1 \times 10^{-5}$ Pa) for 3 h at 423 K. The specific surface area was calculated by the Brunauer–Emmett–Teller (BET) equation. The pore size and pore size distribution were derived from the adsorption isotherm branch using the Barrett–Joyner–Halenda (BJH) method. FT-IR spectra were recorded in the range of 4000–400 cm$^{-1}$ on a TENSOR II FT-IR spectrophotometer (Bruker, Germany) at 2 cm$^{-1}$ resolution by an accumulation of 32 scans. Solid samples were prepared by the KBr pellet method and Sandalore by the liquid film method. To examine the interaction of SA with PDA, the two were mixed in nearly equal quantities in liquid paraffin and ground, then coated on the KBr pellet to measure the IR spectra. X-ray photoelectron spectroscopy (XPS) was applied to analyze the chemical composition of nanoparticle surfaces. The analyzer (PerkinElmer, USA) was utilized a monochromatic Al Kα X-ray source (1486.6 eV).

### 2.5. General procedure for irradiation and cumulative release profiles

To examine the photothermal performance of the nanoparticles (NPs), the samples were examined by measuring the temperature changes under a sunlight simulator or a daylight lamp. Briefly, the powder sample (10 mg) was heaped into a thin layer (∼1 0 × 10 × 1 mm³) on a piece of paper and then irradiated for 5 min (environment temperature = 26 °C). The light power was measured by a radiometer (CEL-FZ-A, Au-light Co., Ltd, Beijing). The changes in temperature at the sample surface were recorded in real-time by using a thermal infrared camera (FLIR C2, USA).

Given that the vapor pressure of Sandalore is too low at ambient temperature to meet the sampling requirements of headspace gas chromatography,[35] fragrance release was studied by TGA combining with elemental analysis (EA). In the tests, ∼5 mg samples were taken at regular intervals to analyze the amount of fragrance residue following the method for the loading content of SA (see the ESI†), and the released amount was calculated accordingly. Each release experiment was independently carried out three times and the data were presented as mean ± standard deviation. The method of sample preparation was the same as that in the photothermal measurement described above.

### 2.6. Surface deposition of NPs on substrates and washing durability test

One silk sheet (15.0 mg, *ca.* 1.3 cm × 1.3 cm; purchased from Hangzhou Wensli Co. Ltd., China, prewashed with deionized water) was immersed in a 5 mL of NP dispersion of 0.1 mg mL$^{-1}$ (the total solid content $w_t$ = 0.5 mg) and allowed the incubation for 1 h at room temperature with gentle agitation. Similarly,

another silk sheet, serving as the reference, was treated in the same way without adding NPs. These samples were taken out, dried and quantitatively analyzed by TGA to get the mass of NPs deposited onto fabrics ($w_d$). The percentage deposition of particles was calculated as follows: % deposition = $w_d/w_t \times 100$.

A washing durability test was performed following a previously reported procedure.[36] The NP-treated silk samples were soaked in a ∼5% aqueous solution of neutral liquid detergent (Bluemoon®, Guangzhou, China) with gentle agitation. Five minutes of washing was considered a cycle. After each washing and drying, the samples were observed by the scanning electron microscope. The ratio of the number of residual particles after washing to the number of initial particles deposited on the silk sheets was defined as the particle retention rate, which was used to evaluate the washing durability. The number of NPs deposited on the fabric surface was determined based on SEM images. All measurements, whether deposition or washing durability tests, were conducted in triplicates on two independent silk substrates.

## 3. Results and discussion

### 3.1. Preparation and characterization of silica nanoparticles loading Sandalore

As illustrated in Fig. 1, the employed protocol involves the synthesis of mesoporous silica nanoparticles (MSNs) by a general method[34] followed by immersion in an ethanol solution of Sandalore (SA) and surface modification *via* the *in situ* self-polymerization of dopamine in a weakly alkaline medium.[32,37] The resulting nanocomposites were denoted as SA$_x$/MSN@PDA$_y$ to indicate their composition when necessary, where $x$ is equal to the fragrance loading content (LC) defined above and $y$ represents the mass percent of PDA layer relative to silica. The amount of PDA deposited on the particle surface could be easily regulated by changing the monomer feed ratio in the polymerization stage.

Table 1 summarizes the characterization data of as-prepared nanoparticles (NPs), including the blank samples for control experiments, *i.e.*, fragrance-loaded MSNs without PDA coating (SA$_{46}$/MSN) and PDA-modified unloaded ones (MSN@PDA$_{12.5}$). The results showed that a high encapsulation efficiency (98.4%) can be achieved by impregnating MSNs with SA of the same mass in ethanol solution (entry 2). In this case, the control particle possessed excellent adsorption capacity (460 mg g$^{-1}$), which is equivalent to ∼85% by weight of SA to the silica matrix. For PDA-coated NPs, the loading content (43–48 wt%, entries 3–5) was closed to that of their precursor SA$_{46}$/MSN, and the final encapsulating efficiency reaching up to 77.5–95.7%. The high loading efficiency can be attributed to the excellent adsorption capability of the mesoporous matrix and the interaction of PDA layer with entrapped molecules.[37–42]

DLS measurements showed that the average hydrodynamic size of the bare MSNs and SA$_{46}$/MSN was approximately 100 nm in diameter (entries 1 and 2), while that of NPs with PDA coating was in the range of 120–140 nm (entries 3–6). Scanning electron microscopy (SEM) images of these samples revealed well-distributed particles of sizes consistent with those obtained
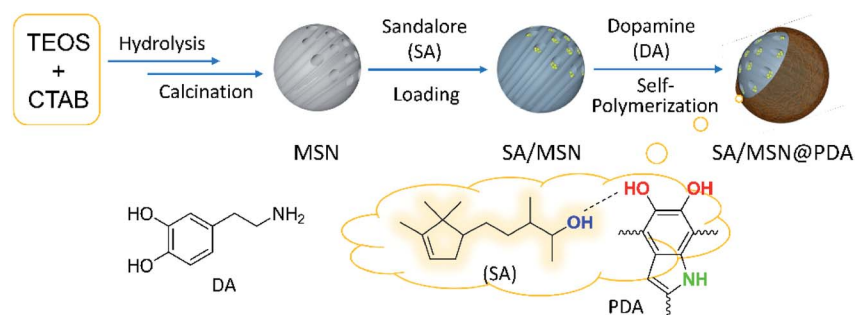
Fig. 1 Illustration showing the fabricating process of Sandalore-loaded nanocomposites $SA_x/MSN@PDA_y$ as well as the proposed hydrogen-bonding interaction of SA with the structural motif in the polymer network.

by DLS (Fig. S1 in the ESI†). Compared with pure MSNs, the relatively large size of PDA-modified particles may be contributed to the polymer shell forming around their surface. The ζ-potential was −16.9 mV ± 0.4 for the MSNs, owing to the presence of negatively charged silanol groups.[40] After PDA modification, the ζ value slightly increased to −16.5 to −13.1 mV (entries 3–6), indicating a decrease in free silanol density on the particle surface.[37,41]

Transmission electron microscopy (TEM) studies were performed to access the morphology of the NPs. As can be seen in Fig. 2A and B, all the NPs presented a nearly spherical shape and well-ordered hexagonal structure with uniform pore sizes.[44] $SA_{48}/MSN@PDA_{5.3}$ displayed a distinct shell on the particle periphery, and thus had a larger size as compared to the pristine MSNs, which was in accord with DLS measurements (Fig. 2C).

The successful deposition of PDA film onto the silica surface was also confirmed by XPS analysis. As shown in Fig. 2D, all of PDA-coated NPs exhibited a typical N1s signal at the binding energy of ∼400 eV in XPS spectra,[28,42,43] but bare MSNs did not. Furthermore, the enhancement of the N1s peak for the samples corresponds to the decrease of the Si2p signal at around 103.5 eV (Fig. 2E), which are in concert with their PDA contents. These observations demonstrated the existence of PDA coating.

Fig. 3A and B present $N_2$ adsorption–desorption isotherms and the corresponding BJH pore size distribution of the NPs. It was observed that MSNs displayed a typical IVb isotherm.[45] The BET surface area, pore volume and pore size of MSNs were

measured as 1072.7 m$^2$ g$^{-1}$, 1.3688 cm$^3$ g$^{-1}$ and about 2.58 nm, respectively. After loading the fragrance, the specific surface area dropped sharply to 23.3 m$^2$ g$^{-1}$ ($SA_{46}/MSN$), and further to 20.0 m$^2$ g$^{-1}$ for $SA_{43}/MSN@PDA_{3.9}$. Nitrogen isotherms showed the expected nitrogen uptake only at high $p/p_0 = 0.95$–1.0. Their pore volume and pore size were too small to be determined. This suggests that the fragrance molecules occupied the mesoporous channels of silica matrices,[37] and that the PDA layer effectively obstructed the entrance of the channels in agreement with TEM observation (Fig. 2B).

Infrared spectroscopy was employed to investigate the surface chemistry changes along with the formation of composite nanoparticles. The characteristic peaks of $SiO_2$, SA, and the molecular chains of PDA, such as Si–O–Si, O–H, N–H, and aromatic ring, were identified in Fig. S5 (see the ESI†), demonstrating that the fragrance and PDA were conjugated to MSNs.

It is worth commenting that a strongly attached PDA film can be formed on the surfaces in a slightly alkaline aqueous condition (pH = 8.5).[20,21] During the self-polymerization, dopamine is oxidized by oxygen to dopamine quinone, which then further reacts with amines and other catechols/quinones to yield PDA.[25] The polar 5,6-dihydroxyindole motif in the polymer skeleton has the potential to interact through hydrogen bonding with the entrapped molecules in the matrix.[38] As seen by comparing the IR spectra in Fig. 3C, SA shows a broad absorption band centered at 3366 cm$^{-1}$ and a weak peak at

Table 1 Characterization of prepared nanoparticles

| Entry | Samples[a] | EE[b] (%) | Size[c] (nm) | | ζ potential (mV) |
|---|---|---|---|---|---|
| | | | DLS | SEM | |
| 1 | MSNs | N/A[d] | 102.4 ± 54.6 | 107.5 ± 13.9 | −16.9 ± 0.4 |
| 2 | $SA_{46}/MSN$ | 98.4 ± 0.8 | 99.9 ± 43.1 | 110.1 ± 13.7 | −17.1 ± 0.2 |
| 3 | $SA_{47}/MSN@PDA_{1.1}$ | 90.8 ± 0.8 | 118.7 ± 27.4 | 107.8 ± 9.1 | −16.5 ± 0.5 |
| 4 | $SA_{43}/MSN@PDA_{3.9}$ | 88.0 ± 7.1 | 124.9 ± 32.0 | 109.5 ± 9.8 | −15.0 ± 0.6 |
| 5 | $SA_{48}/MSN@PDA_{5.3}$ | 96.6 ± 6.0 | 141.4 ± 44.2 | 118.1 ± 13.7 | −13.1 ± 0.5 |
| 6 | $MSN@PDA_{12.5}$ | N/A[d] | 139.5 ± 29.4 | 109.3 ± 10.1 | −15.0 ± 0.4 |

[a] Loading contents of SA and PDA were determined by TGA and EA; see Table S1 in the ESI for details. [b] Encapsulating efficiency (mean ± standard deviation, $n = 3$). [c] See Fig. S1–S3 in the ESI. [d] N/A = not applicable.
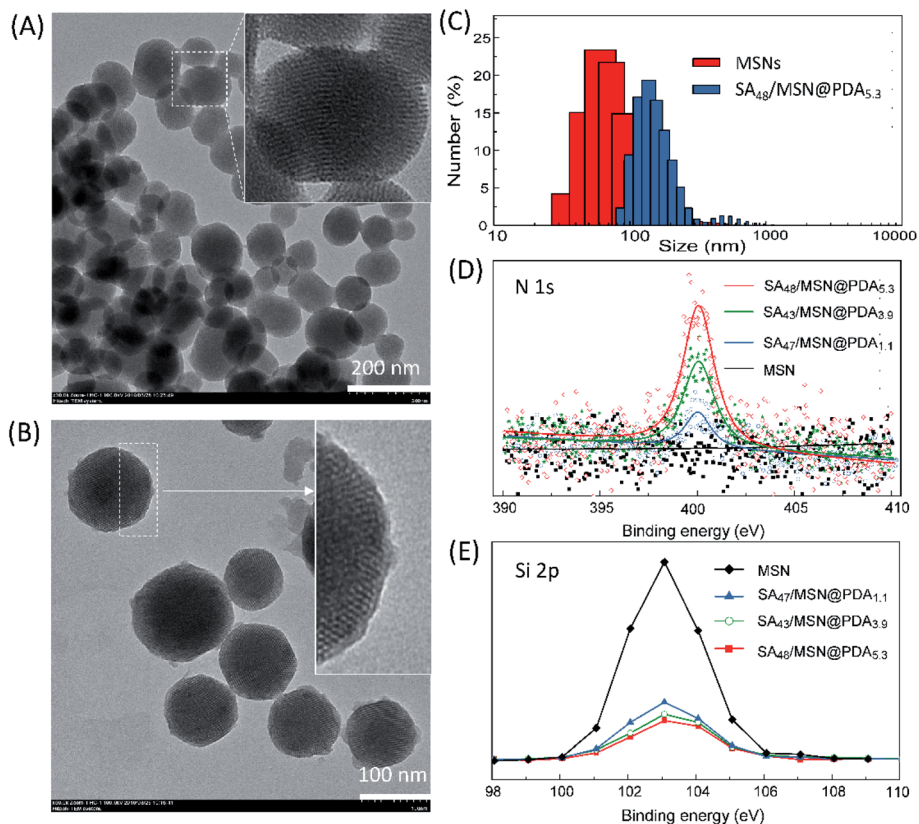
Fig. 2 TEM images of pristine MSNs (A) and SA$_{48}$/MSN@PDA$_{5.3}$ (B), and their corresponding particle size distributions (C) obtained from DLS measurements (Fig. S1†). (D and E) XPS spectra of MSNs, SA$_{47}$/MSN@PDA$_{1.1}$, SA$_{43}$/MSN@PDA$_{3.9}$, and SA$_{48}$/MSN@PDA$_{5.3}$ (the wide scan survey is given in Fig. S4†).
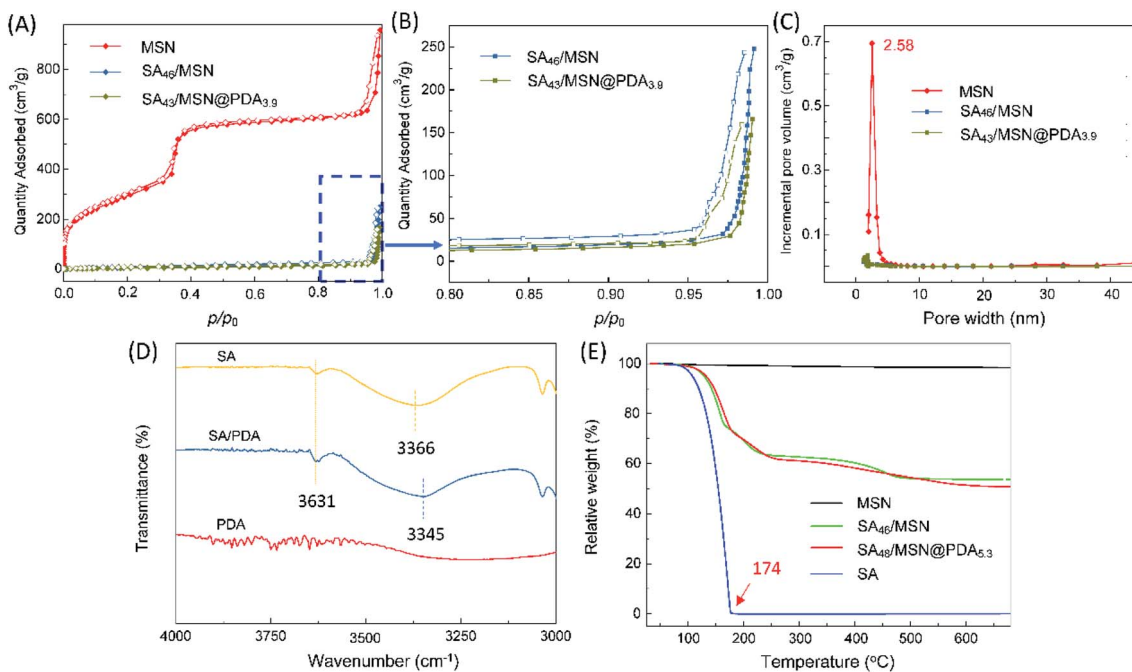


Fig. 3 (A) BET nitrogen adsorption–desorption isotherms of MSNs, SA$_{46}$/MSN, and SA$_{43}$/MSN@PDA$_{3.9}$ at 77 K. (B) The corresponding magnified view of the high $p/p_0$ region for the latter two samples. Solid and hollow points represent adsorption and desorption data, respectively. (C) BJH pore size distribution profiles. (D) Expanded FTIR of SA, PDA, SA/PDA blend in paraffin from 3000 to 4000 cm$^{-1}$. (E) TGA curves of SA, MSNs, SA$_{46}$/MSN, and SA$_{48}$/MSN@PDA$_{5.3}$.

$3631~cm^{-1}$, which are assignable respectively to the associated and free hydroxyl groups in the molecules.[46] Upon blending with PDA in paraffin, a clear shift in the maximum of the associated hydroxyl band has been seen from 3366 to $3345~cm^{-1}$, whereas the free hydroxyl peak remained unchanged. One possible explanation for this is that the catechol moieties of PDA, as a more competitive hydrogen bonding donor/acceptor than the SA's hydroxyl groups, formed stronger hydrogen bonding with the odorant molecules (see Fig. 1) and thus resulted in a downward shift of the absorption band.[26,32,33] Undoubtedly, such intermolecular interactions would be favorable for the retention of spices in matrices and sustainable release as well.

Fig. 3D depicts the thermal gravimetric analysis (TGA) curves, which could be used to determine the amounts of PDA coating and entrapped SA (Table 1). The weight loss of bare MSNs was less than 1.5% from 25 to 680 °C, attributed to desorption of physically adsorbed water; whereas the neat SA fully evaporates before 174 °C. In the case of PDA-coated NPs, the mass decline exhibited a multi-step process. The weight loss before 250 °C was mainly due to the volatilization of the spice, while over this point could be ascribed to the decomposition of the PDA coating.[28]

## 3.2. The photothermal effect and fragrance release behavior of nanocomposites

The photothermal conversion capability of PDA-functionalized NPs was studied with respect to the sample $SA_{46}/MSN$ that does not contain PDA as a control. Upon the simulated sunlight irradiation for ~90 s at $100~mW~cm^{-2}$, the temperature of all the NPs rose to their respective maximum, as shown in Fig. 4A. Among them, the constant temperature plateau appeared after the composite $SA_{48}/MSN@PDA_{5.3}$ being heated to ~60 °C, while for the control the temperature only reached 36 °C under the same conditions. From Fig. 4B, the temperature of $SA_{48}/MSN@PDA_{5.3}$ was elevated from 26 °C to 68 °C in 60 s under irradiation of $150~mW~cm^{-2}$. However, almost no temperature change was detected for the sample in the case of indoor lighting ($<1~mW~cm^{-2}$). The dependence of the photothermal heating effect on the PDA content, irradiation intensity and

duration is similar to previously reported results.[29,47] Once removal of the irradiation, the temperature of composites dropped instantly. Such a heating/cooling switching modulated by light can be cycled repeatedly without an obvious decrease in the maximum temperature (Fig. S6†), indicating that these nanocomposites possessed promising photothermal stability and temperature regulation ability.

Subsequently, the fragrance release behavior of these composites upon variation of both the PDA content and irradiation power was studied at ambient temperature (26 °C). As a control experiment, we first examined the fragrance release in the case of no illumination (Fig. 5A). Overall, all the NPs, with or without PDA coating, exhibited a fairly slow, but nearly linear release profile as the neat SA oil. However, it is noteworthy that the fragrance entrapped in the MSNs exhibited a greater tendency to volatilize than its bulk state ($SA_{46}/MSN$ *vs.* SA), especially on exposure to light (Fig. 5B). A reasonable explanation is that the porous matrix increases the vapor–liquid interfacial area of the adsorbed Sandalore and leads to accelerated aroma vaporization. Compared to the reference sample $SA_{46}/MSN$, the PDA coated particles ($SA_{47}/MSN@PDA_{1.1}$ and $SA_{48}/MSN@PDA_{5.3}$) released far less fragrance in the absence of irradiation. Over the 15 day observation period, the former had a cumulative release degree of 48%, while the latter two were approximately 16% and 12%, respectively. The results indicated that the PDA coating does act as a protective film, which is similar to some drug delivery systems.[28,30,31,47]

From Fig. 5B and C, the release of fragrances from PDA-modified NPs was significantly facilitated when exposed to the simulated sunlight, whereas for the sample $SA_{46}/MSN$ the release rate increased much less. It can be found that the increased cumulative release of fragrances upon increasing the amount of PDA or irradiation intensity is consistent with the temperature variation of the composites shown in Fig. 4. For the sample $SA_{48}/MSN@PDA_{5.3}$, the total fraction of fragrance liberated from the nanoparticles achieved ~85% on exposure to $150~mW~cm^{-2}$ for 8 h. Under the diffuse sunlight through a nearby window (~$50~mW~cm^{-2}$), the escaped amount of SA was about 35%. However, the fragrance release was barely detectable with exposure to the indoor illumination or low
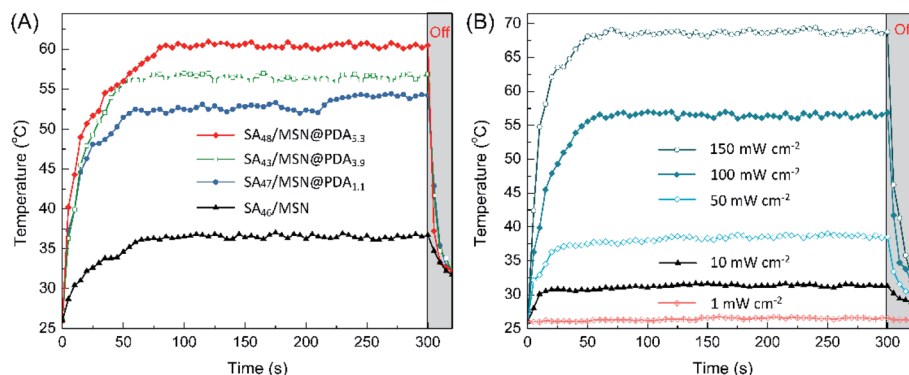


Fig. 4 Temperature elevation of (A) the NPs under the simulated sunlight ($100~mW~cm^{-2}$) and (B) $SA_{48}/MSN@PDA_{5.3}$ as a function of irradiation duration at various power intensities.
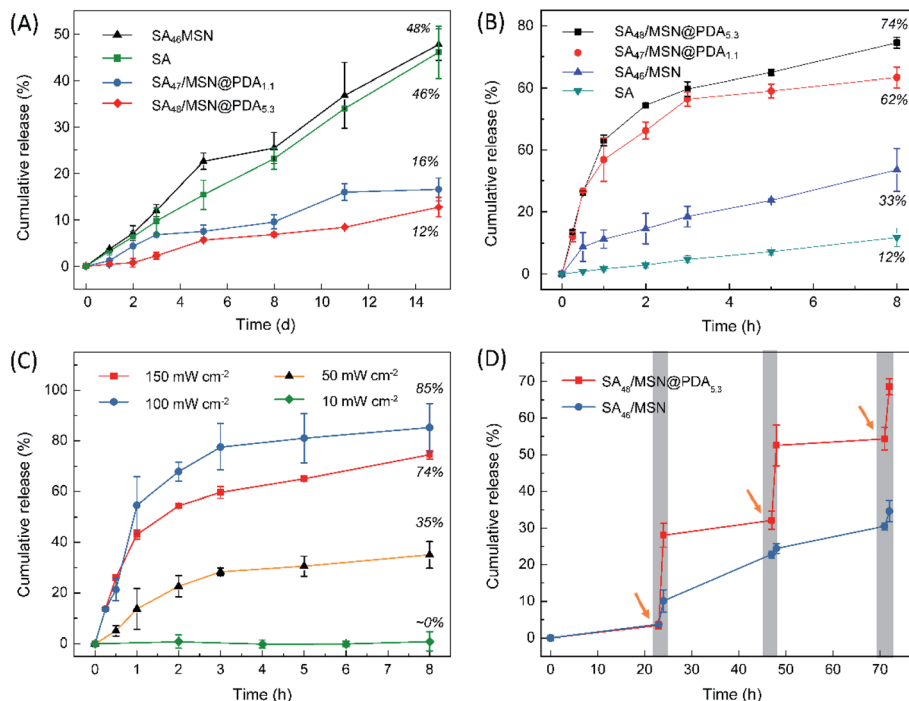
**Fig. 5** (A) Time-elapsed fragrance release profiles of the neat SA and SA-loaded NPs in the dark and (B) under simulated sunlight irradiation of 100 mW cm$^{-2}$. (C) Release curves of SA$_{48}$/MSN@PDA$_{5.3}$ under the simulated sunlight with different irradiation intensity. (D) Time-dependent release of Sandalore from SA$_{48}$/MSN and SA$_{48}$/MSN@PDA$_{5.3}$ particles. The arrow indicates the time at which the simulated sunlight (100 mW cm$^{-2}$) was turned on. The samples were exposed to light for 1 h and then kept in the dark for 23 h.

irradiation (1–10 mW cm$^{-2}$). As a result, with the dual function of PDA coating, the release of fragrances can be controlled by adjusting the light power, and even realize the aroma ON–OFF switching effect (Fig. 5D). The release acceleration is ascribed to the photothermal effect of the PDA layer, which could elevate the local temperature under light irradiation and thus drive molecular desorption through the thermal movement of the crystalline lattice.[29,47]
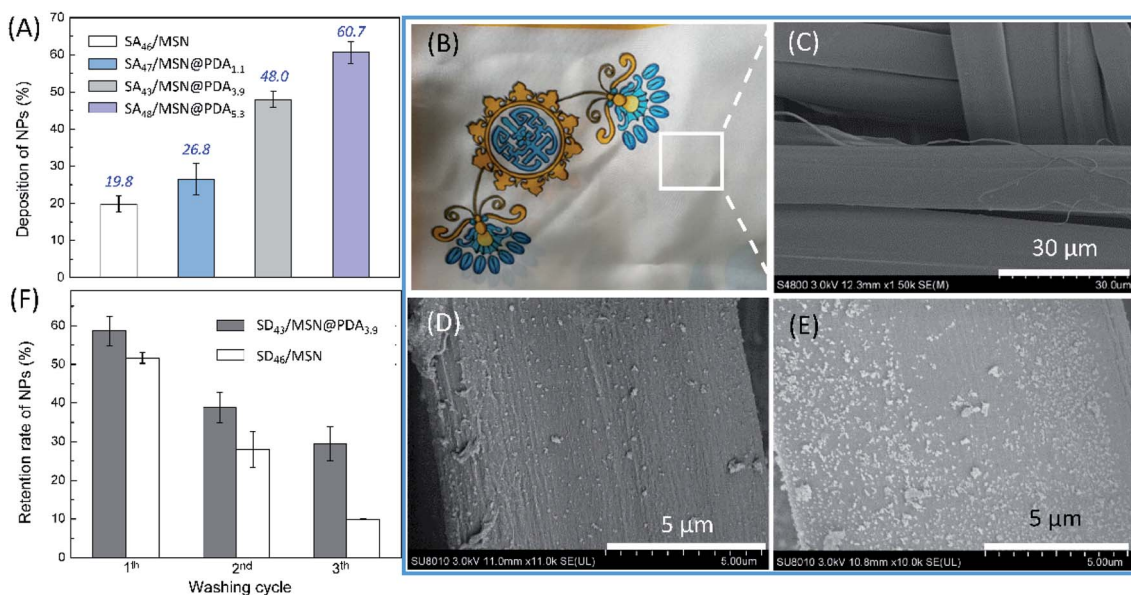


**Fig. 6** (A) Percentage deposition of NPs (0.1 mg mL$^{-1}$) onto silk scarves. (B) Photograph and (C) SEM image of the pristine silk sample. SEM images of silk scarves after deposition of (D) SA$_{46}$/MSN and (E) SA$_{48}$/MSN@PDA$_{5.3}$. (F) Change in the retention of nanoparticles deposited on the silk surface with washing cycles (5 min for each washing). The retention percentage was estimated by the variation in the particle number in SEM images. Error bars represent the standard deviation of three independent measurements.

### 3.3. Deposition of NPs on the fabric surface

The surface deposition of fragranced products is an important parameter that determines the long-lastingness of fragrance perception.[48–50] We thus examined the adhesion of fragrance-loaded nanoparticles to the silk fabric and their washing durability. Fig. 6A shows the results of deposition experiments, where the deposition efficiency was measured following the incubation of a 0.1 mg mL$^{-1}$ of NP dispersion to ~15 mg of silk scarves (1.3 cm × 1.3 cm, see: Section 2.6). As expected, the affinity of NPs toward the target substrate strongly depends on the presence of PDA coating and its content.[21] Specifically, the extent of deposition of the control SA$_{46}$/MSN on the silk scarf was about 19.8%, while the introduction of 1.1 wt% PDA coating increased the deposition to 26.8% (SA$_{47}$/MSN@PDA$_{1.1}$). Further enhancing the PDA content to 3.9 wt% and 5.3 wt% resulted in 48.0% (SA$_{43}$/MSN@PDA$_{3.9}$) and 60.7% (SA$_{48}$/MSN@PDA$_{5.3}$) deposition, respectively.

The enhanced surface deposition of PDA-coated NPs can also be intuitively judged from Fig. 6B–E. Fig. 6B and C show optical and SEM pictures of the silk scarf before treatment with NPs, and Fig. 6D and E are the SEM images of the fabric incubated in dispersions containing SA$_{46}$/MSN and SA$_{48}$/MSN@PDA$_{3.9}$, respectively. As could be seen by comparing the images in Fig. 6D and E, the distribution of SA$_{48}$/MSN@PDA$_{3.9}$ on the fiber surface was denser than that of SA$_{46}$/MSN after impregnating in the same way, consistent with the results of deposition experiments.

Finally, the adhesion of NPs to the silk surface was investigated *via* washing tests. As a representative, Fig. 6F compares the washing durability of SA$_{47}$/MSN@PDA$_{3.9}$ and SA$_{46}$/MSN deposited on the fabric under conditions that emulate the use in laundry applications (see: Section 2.6). It was found that at the end of each washing cycle (5 min for each washing), the retention percentage of SA$_{47}$/MSN@PDA$_{3.9}$ particles was always higher than that of the control. This in turn indicates an effective deposition of the PDA-modified nanocarriers on the silk under the here-described conditions. After three times of washing, the two particles retained around 30% and 10% of their initial deposition, respectively. The results combined with the deposition experiments highlight another positive effect of the PDA coating is the presence of polar groups like catechol moieties, which enhanced the adhesion ability of PDA-modified NPs,[20,21,51] and this would contribute to the long-lasting release of aroma.

## 4. Conclusions

In summary, we developed a kind of photothermo-responsive nanocarriers for the controlled delivery of low-volatile synthetic odorant Sandalore. Benefiting from the individual merits of MSNs and PDA, the as-prepared composites featured high loading capacity (430–480 mg g$^{-1}$) and a light-modulated aroma release behavior. In the dark or upon weak illumination, the fragrance was tightly entrapped in the matrix, while its release can be effectively exerted by the simulated sunlight-induced photothermal heating in a switchable manner.

Additionally, the PDA coating also bestows the nanocomposites with a strong affinity to the silk fabric, resulting in higher deposition efficiency (up to ~61%) and washing resistance as compared to the control particles without PDA functionalization. It is worth noting that the photothermally responsive release mechanism is desirable or more flexible in certain application scenarios because it allows the aroma release to be controlled by light irradiation rather than directly heating. Although more work remains to be done to improve the applicability of the multifunctional fragrance-loaded composites, the present study offered a simple but reliable strategy for the construction of controlled fragrance-release systems.

## Conflicts of interest

There are no conflicts of interest to declare.

## Acknowledgements

## Notes and references

1 R. E. Naipawer and W. M. Easter, 3-Methyl-5-(2,2,3-trimethylcyclopent-3-en-1-yl)pentan-2-ol compound and perfume compositions, *US Pat.* 4052341, 1977.
2 H. Panda, *Cultivation and utilization of aromatic plants*, Asia Pacific Business Press Inc., New Delhi, 2005, pp. 218–219.
3 A. B. Camps, *Perfumery: Techniques in evolution*, Lulu, Morrisville, 2nd edn, 2017, p. 82.
4 D. Busse, P. Kudella, N. M. Grüning, G. Gisselmann, S. Ständer, T. Luger, F. Jacobsen, L. Steinsträßer, R. Paus, P. Gkogkolou, M. Böhm, H. Hatt and H. Benecke, A synthetic sandalwood odorant induces wound-healing processes in human keratinocytes via the olfactory receptor OR2AT4, *J. Invest. Dermatol.*, 2014, **134**, 2823–2832, DOI: 10.1038/jid.2014.273.
5 J. Chéret, M. Bertolini, L. Ponce, J. Lehmann, T. Tsai, M. Alam, H. Hatt and R. Paus, Olfactory receptor OR2AT4 regulates human hair growth, *Nat. Commun.*, 2018, **9**, 1–12, DOI: 10.1038/s41467-018-05973-0.
6 T. Pluskal and J. Weng, Natural product modulators of human sensations and mood: molecular mechanisms and therapeutic potential, *Chem. Soc. Rev.*, 2018, **47**, 1592–1637, DOI: 10.1039/c7cs00411g.
7 The vapor pressure was acquired from Scifinder, which deduced by the *Advanced Chemistry Development (ACD/Labs) Software Version 11.02*, 1994–2013.
8 A. E. Edris and M. A. S. A. El-Galeel, Solubilization of some flavor and fragrance oils in surfactant/water system, *World Appl. Sci. J.*, 2010, **8**, 86–91.
9 L. He, J. Hu and W. Deng, Preparation and application of flavor and fragrance capsules, *Polym. Chem.*, 2018, **9**, 4926–4946, DOI: 10.1039/c8py00863a.

10 Z. Zhou, J. Hu, L. Jiang, W. Zhu, X. Zhang, Z. Xiao and Y. Shen, Nanotechnology in fragrances: current status and future prospects, *Sci. Sin.: Chim.*, 2019, **49**, 575–580, DOI: 10.1360/N032018-00168.

11 J. Seemork, T. Tree-Udom and S. Wanichwecharungruang, A refillable fragrance carrier with a tuneable thermal switch, *Flavour Fragrance J.*, 2012, **27**, 386–392, DOI: 10.1002/ffj.3116.

12 I. Hofmeister, K. Landfester and A. Taden, pH-Sensitive nanocapsules with barrier properties: fragrance encapsulation and controlled release, *Macromolecules*, 2014, **47**, 5768–5773, DOI: 10.1021/ma501388w.

13 Y. Liu, Y. Wang, J. Huang, Z. Zhou, D. Zhao, L. Jiang and Y. Shen, Encapsulation and controlled release of fragrances from functionalized porous metal-organic frameworks, *AIChE J.*, 2019, **65**, 491–499, DOI: 10.1002/aic.16461.

14 R. Ciriminna and M. Pagliaro, Sol-gel microencapsulation of odorants and flavors: opening the route to sustainable fragrances and aromas, *Chem. Soc. Rev.*, 2013, **42**, 9243–9250, DOI: 10.1039/c3cs60286a.

15 F. L. Sousa, M. Santos, S. M. Rocha and T. Trindade, Encapsulation of essential oils in $SiO_2$ microcapsules and release behavior of volatile compounds, *J. Microencapsulation*, 2014, **31**, 627–635, DOI: 10.3109/02652048.2014.911376.

16 G. M. Radulova, T. G. Slavova, P. A. Kralchevsky, E. S. Basheva, K. G. Marinova and K. D. Danov, Encapsulation of oils and fragrances by core-in-shell structures from silica particles, polymers and surfactants: the brick-and-mortar concept, *Colloids Surf., A*, 2018, **559**, 351–364, DOI: 10.1016/j.colsurfa.2018.09.079.

17 P. Wang, Y. Zhu, X. Yang and A. Chen, Prolonged-release performance of perfume encapsulated by tailoring mesoporous silica spheres, *Flavour Fragrance J.*, 2008, **23**, 29–34, DOI: 10.1002/ffj.

18 Z. Cao, C. Xu, X. Ding, S. Zhu, H. Chen and D. Qi, Synthesis of fragrance/silica nanocapsules through a sol-gel process in miniemulsions and their application as aromatic finishing agents, *Colloid Polym. Sci.*, 2015, **293**, 1129–1139, DOI: 10.1007/s00396-015-3502-2.

19 Z. Lu, T. Zhang, J. Shen, Z. Xiao, J. Hu, Y. Niu, D. Yu, L. Chen and X. Zhang, Effects of fragrance-loaded mesoporous silica nanocolumns on the central nervous system, *J. Biomed. Nanotechnol.*, 2018, **14**, 1578–1589, DOI: 10.1166/jbn.2018.2607.

20 H. Lee, S. M. Dellatore, W. M. Miller and P. B. Messersmith, Mussel-inspired surface chemistry for multifunctional coatings, *Science*, 2007, **318**, 426–430, DOI: 10.1126/science.1147241.

21 H. Lee, J. Rho and P. B. Messersmith, Facile conjugation of biomolecules onto surfaces via mussel adhesive protein inspired coatings, *Adv. Mater.*, 2009, **21**, 431–434, DOI: 10.1002/adma.200801222.

22 L. S. Lin, Z. X. Cong, J. B. Cao, K. M. Ke, Q. L. Peng, J. Gao, H. H. Yang, G. Liu and X. Chen, Multifunctional $Fe_3O_4$@polydopamine core-shell nanocomposites for intracellular mRNA detection and imaging-guided photothermal therapy, *ACS Nano*, 2014, **8**, 3876–3883, DOI: 10.1021/nn500722y.

23 X. Liu, J. Cao, H. Li, J. Li, Q. Jin, K. Ren and J. Ji, Mussel-inspired polydopamine: a biocompatible and ultrastable coating for nanoparticles in vivo, *ACS Nano*, 2013, **7**, 9384–9395, DOI: 10.1021/nn404117j.

24 Y. Liu, K. Ai, J. Liu, M. Deng, Y. He and L. Lu, Dopamine-melanin colloidal nanospheres: an efficient near-infrared photothermal therapeutic agent for in vivo cancer therapy, *Adv. Mater.*, 2013, **25**, 1353–1359, DOI: 10.1002/adma.201204683.

25 Y. Liu, K. Ai and L. Lu, Polydopamine and its derivative materials: synthesis and promising applications in energy, environmental, and biomedical fields, *Chem. Rev.*, 2014, **114**, 5057–5115, DOI: 10.1021/cr400407a.

26 R. S. Ambekar and B. Kandasubramanian, A polydopamine-based platform for anti-cancer drug delivery, *Biomater. Sci.*, 2019, **7**, 1776–1793, DOI: 10.1039/c8bm01642a.

27 W. Cheng, X. Zeng, H. Chen, Z. Li, W. Zeng, L. Mei and Y. Zhao, Versatile polydopamine platforms: synthesis and promising applications for surface modification and advanced nanomedicine, *ACS Nano*, 2019, **13**, 8537–8565, DOI: 10.1021/acsnano.9b04436.

28 D. Zhu, C. Hu, Y. Liu, F. Chen, Z. Zheng and X. Wang, Enzyme-/redox-responsive mesoporous silica nanoparticles based on functionalized dopamine as nanocarriers for cancer therapy, *ACS Omega*, 2019, **4**, 6097–6105, DOI: 10.1021/acsomega.8b02537.

29 Y. Xing, J. Zhang, F. Chen, J. Liu and K. Cai, Mesoporous polydopamine nanoparticles with co-delivery function for overcoming multidrug resistance via synergistic chemo-photothermal therapy, *Nanoscale*, 2017, **9**, 8781–8790, DOI: 10.1039/c7nr01857f.

30 W. Tao, X. W. Zeng, J. Wu, X. Zhu, X. H. Yu, X. D. Zhang, J. X. Zhang, G. Liu and L. Mei, Polydopamine-based surface modification of novel nanoparticle-aptamer bioconjugates for *in vivo* breast cancer targeting and enhanced therapeutic effects, *Theranostics*, 2016, **6**, 470–484, DOI: 10.7150/thno.14184.

31 J. Park, T. F. Brust, H. J. Lee, S. C. Lee, V. J. Watts and Y. Yeo, Polydopamine-based simple and versatile surface modification of polymeric nanodrug carriers, *ACS Nano*, 2014, **8**, 3347–3356, DOI: 10.1021/nn405809c.

32 L. Yang, Z. Wang, G. Fei and H. Xia, Polydopamine particles reinforced poly(vinyl alcohol) hydrogel with NIR light triggered shape memory and self-healing capability, *Macromol. Rapid Commun.*, 2017, **38**, 1–8, DOI: 10.1002/marc.201700421.

33 Y. Xu, P. Wu, P. Feng, W. Guo, W. Yang and C. Shuai, Interfacial reinforcement in a poly-*l*-lactic acid/mesoporous bioactive glass scaffold via polydopamine, *Colloids Surf., B*, 2018, **170**, 45–53, DOI: 10.1016/j.colsurfb.2018.05.065.

34 C. Park, K. Lee and C. Kim, Photoresponsive cyclodextrin-covered nanocontainers and their sol-gel transition induced by molecular recognition, *Angew. Chem., Int. Ed.*, 2009, **48**, 1275–1278, DOI: 10.1002/anie.200803880.

35 A. Trachsel, C. Chapuis and A. Herrmann, Slow release of fragrance aldehydes and ketones in functional perfumery from dynamic mixtures generated with *N*-heteroarylmethyl-substituted secondary diamines, *Flavour Fragrance J.*, 2013, **28**, 280–293, DOI: 10.1002/ffj.3170.

36 L. Ye, Z. Li, R. Niu, Z. Zhu, Y. Shen and L. Jiang, All-aqueous direct deposition of fragrance-loaded nanoparticles onto fabric surfaces by electrospraying, *ACS Appl. Polym. Mater.*, 2019, **1**, 2590–2596, DOI: 10.1021/acsapm.9b00457.

37 W. Cheng, C. Liang, L. Xu, G. Liu, N. Gao, W. Tao, L. Luo, Y. Zuo, X. Wang, X. Zhang, X. Zeng and L. Mei, TPGS-functionalized polydopamine-modified mesoporous silica as drug nanocarriers for enhanced lung cancer chemotherapy against multidrug resistance, *Small*, 2017, **13**, 1–12, DOI: 10.1002/smll.201700623.

38 F. Bernsmann, V. Ball, F. Addiego, A. Ponche, M. Michel, J. Gracio, V. Toniazzo and D. Ruch, Dopamine-melanin film deposition depends on the used oxidant and buffer solution, *Langmuir*, 2011, **27**, 2819–2825, DOI: 10.1021/la104981s.

39 P. Zhou, F. Wu, T. Zhou, X. Cai, S. Zhang, X. Zhang, Q. Li, Y. Li, Y. Zheng, M. Wang, F. Lan, G. Pan, D. Pei and S. Wei, Simple and versatile synthetic polydopamine-based surface supports reprogramming of human somatic cells and long-term self-renewal of human pluripotent stem cells under defined conditions, *Biomaterials*, 2016, **87**, 1–17, DOI: 10.1016/j.biomaterials.2016.02.012.

40 I. Slowing, B. G. Trewyn and V. S. Y. Lin, Effect of surface functionalization of MCM-41-type mesoporous silica nanoparticles on the endocytosis by human cancer cells, *J. Am. Chem. Soc.*, 2006, **128**, 14792–14793, DOI: 10.1021/ja0645943.

41 D. Chang, Y. Gao, L. Wang, G. Liu, Y. Chen, T. Wang, W. Tao, L. Mei, L. Huang and X. Zeng, Polydopamine-based surface modification of mesoporous silica nanoparticles as pH-sensitive drug delivery vehicles for cancer therapy, *J. Colloid Interface Sci.*, 2016, **463**, 279–287, DOI: 10.1016/j.jcis.2015.11.001.

42 Y. Wei, L. Gao, L. Wang, L. Shi, E. Wei, B. Zhou, L. Zhou and B. Ge, Polydopamine and peptide decorated doxorubicin-loaded mesoporous silica nanoparticles as a targeted drug delivery system for bladder cancer therapy, *Drug Delivery*, 2017, **24**, 681–691, DOI: 10.1080/10717544.2017.1309475.

43 D. M. Eby, K. Artyushkova, A. K. Paravastu and G. R. Johnson, Probing the molecular structure of antimicrobial peptide-mediated silica condensation using X-ray photoelectron spectroscopy, *J. Mater. Chem.*, 2012, **22**, 9875–9883, DOI: 10.1039/c2jm30837a.

44 I. I. Slowing, J. L. Vivero-Escoto, C. W. Wu and V. S.-Y. Lin, Mesoporous silica nanoparticles as controlled release drug delivery and gene transfection carriers, *Adv. Drug Delivery Rev.*, 2008, **60**, 1278–1288, DOI: 10.1016/j.addr.2008.03.012.

45 M. Thommes, K. Kaneko, A. V. Neimark, J. P. Olivier, F. Rodriguez-Reinoso, J. Rouquerol and K. S. W. Sing, Physisorption of gases, with special reference to the evaluation of surface area and pore size distribution (IUPAC Technical Report), *Pure Appl. Chem.*, 2015, **87**, 1051–1069, DOI: 10.1515/pac-2014-1117.

46 J. Coates, Interpretation of infrared spectra, a practical approach, *Encycl. Anal. Chem.*, 2006, pp. 1–23. DOI: 10.1002/9780470027318.a5606.

47 C. Chen, W. Tang, D. Jiang, G. Yang, X. Wang, l. Zhou, W. Zhang and P. Wang, Hyaluronic acid conjugated polydopamine functionalized mesoporous silica nanoparticles for synergistic targeted chemo-photothermal therapy, *Nanoscale*, 2019, **11**, 11012–11024, DOI: 10.1039/c9nr01385g.

48 D. L. Berthier, N. Paret, A. Trachsel and A. Herrmann, Influence of the backbone structure on the release of bioactive volatiles from maleic acid-based polymer conjugates, *Bioconjugate Chem.*, 2010, **21**, 2000–2012, DOI: 10.1021/bc100223s.

49 K. A. Günay, D. L. Berthier, H. A. Jerri, D. Benczédi, H.-A. Klok and A. Herrmann, Selective peptide-mediated enhanced deposition of polymer fragrance delivery systems on human hair, *ACS Appl. Mater. Interfaces*, 2017, **9**, 24238–24249, DOI: 10.1021/acsami.7b06569.

50 K. A. Günay, D. Benczédi, A. Herrmann and H.-A. Klok, Peptide-enhanced selective surface deposition of polymer-based fragrance delivery systems, *Adv. Funct. Mater.*, 2017, **27**, 1603843, DOI: 10.1002/adfm.201603843.

51 B. P. Lee, C.-Y. Chao, F. N. Nunalee, E. Motan, K. R. Shull and P. B. Messersmith, Rapid gel formation and adhesion in photocurable and biodegradable block copolymers with high DOPA content, *Macromolecules*, 2006, **39**, 1740–1748, DOI: 10.1021/ma0518959.